Available online at www.sciencedirect.com
SCIENCE DIRECT®
Thermochimica Acta 425 (2005) 47–57
thermochimica acta
www.elsevier.com/locate/tca

Crystallization kinetics of a multicomponent Fe-based amorphous alloy using modulated differential scanning calorimetry

K.G. Raval [a], Kirit N. Lad [b], Arun Pratap [b,*], A.M. Awasthi [c], S. Bhardwaj [c]

[a] *Electronics Department, Narmada College of Science and Commerce, Zadeshwar, Bharuch 392011, India*
[b] *Applied Physics Department, Faculty of Technology and Engineering, M.S. University of Baroda, Vadodara 390001, India*
[c] *Inter University Consortium for DAE Facilities, Khandwa Road, Indore 452001, India*

Received 21 February 2003; received in revised form 20 May 2004; accepted 26 May 2004
Available online 18 August 2004

Abstract

The kinetics of crystallization of a Fe-based multicomponent metallic glass $Fe_{67}Co_{18}B_{14}Si_1$, commercially known as 2605CO, is studied using modulated differential scanning calorimetry (MDSC) which still remains much less explored for the study of crystallization kinetics. The modified Kissinger equation and the one given by Matusita and Sakka for the non-isothermal crystallization have been employed to analyze the crystallization data at various heating rates. The effect of non-linear heating on the kinetics of crystallization has been discussed. It has been found that the dimensionality of crystallization is heating rate independent in case of DSC while in case of MDSC it is heating rate dependent.

Keywords: Modulated differential scanning calorimetry; Fe-based amorphous alloy; Crystallization kinetics

1. Introduction

Metallic glasses have a combination of amorphous structure and metallic bond providing them a new and unique quality, which cannot be found either in pure metals or in regular glasses. Further, Fe-based metallic glasses have been recognized to possess two important properties, which give them an edge over the crystalline Fe–Si alloy [1–4]. First, a more slender magnetization (hysteresis) loop than grain-oriented Fe–Si and secondly, a higher electrical resistivity reducing induced eddy currents in comparison to crystalline Fe–Si alloy. This has resulted into increased use of wide sheets of Fe-based metallic glasses as transformer laminations. $Fe_{67}Co_{18}B_{14}Si_1$ (2605CO) (procured from the Allied Signal Corporation, USA) is among the family of such glasses. It is also well-known that the amorphous metallic glasses are in non-equilibrium solid state. Therefore, it becomes important to study the factors, which may have crucial bearings on its end applications, related to the amorphous metallic structures. Stability [5] is an important factor related to crystallization, which is generally a thermally activated process of transition from a disordered amorphous structure to an ordered crystal structure. Study of kinetics of crystallization provides E_c, the activation energy of crystallization and parameters like Avrami exponent n, responsible for the mechanism of crystallization. This helps to determine the thermal stability of the metallic glasses. Recently, Galwey [6] has discarded the concept of 'variable activation energies'. Accordingly, activation energy is a physico-chemical parameter determined by the magnitude of the interatomic interactions that are activated and modified during the change occurring. For each particular reaction, it should have a characteristic and constant value. Kaloshkin and Tomilin [7] on the other hand, have given a plausible definition of 'activation energy' with particular reference to crystallization of metallic glasses. The activation energy has been interpreted as a threshold value which if overcome assures the start of the transformation mechanisms. Generally, the crystallization process of a multicomponent amorphous alloy takes place by more than one steps (i.e. by multi-steps). Therefore, the crystallization is not based only on one mechanism, it involves different mechanisms, each one being dominant for a particular step and its range of temperature.

* Corresponding author. Tel.: +91 2652782211; fax: +91 2652423898.
E-mail address: apratapmsu@yahoo.com (A. Pratap).

0040-6031/$ – see front matter © 2004 Elsevier B.V. All rights reserved.
doi:10.1016/j.tca.2004.05.026

Differential scanning calorimetry (DSC) has since long been the most popular technique to study the crystallization process and its kinetics in amorphous materials. However, modulated DSC technique, which is an improvisation over the simple DSC, gives better resolution and sensitivity [8] and yet remains to be checked to its full potential for the same purpose. In the present study, an attempt has been made to determine the utility of this technique to study the kinetics of crystallization.

Temperature modulated differential scanning calorimetry (TMDSC) is a new technique, which is expected to provide unique information not available from conventional DSC by overcoming most of the limitations of conventional DSC. TMDSC is a novel patented [9] and commercialized [10] method and is distinct from the conventional DSC in the sense that, a sinusoidal heating pattern can be superimposed onto an underlying linear heating rate. The slow underlying heating rate is known to improve resolution and more rapid sinusoidal (instantaneous) heating rate improves sensitivity. Thus, the combination of high resolution and sensitivity in the same experiment is one of the unique benefits of modulated DSC.

Numerical modeling and analysis of temperature modulated DSC has been recently carried out [11–13] on the separability of reversing heat flow from non-reversing heat flow to study heat capacity. In fact, one of the major advantages of the MDSC method is its ability to separate these reversing and non-reversible processes by the measurement of the contribution of reverse and non-reserve heat flows in total heat flow during a phase transition. Several studies have been reported for glass transitions and crystallization in polymers [14], chalcogenide glasses [15] and metallic glasses [16] by MDSC. But the study of the detailed crystallization process of amorphous alloy using various kinetics equations is yet to be reported. Our recently reported work [17] on a three component transition metal based amorphous alloy viz. $Ti_{50}Cu_{20}Ni_{30}$ is among the first such publication. Apart from studies of various phase transformations, Cao [12,13] has observed problems in quantitative separation of kinetic and non-kinetic components.

The MDSC technique is not much explored in the area of study of kinetics of crystallization. In the present work, we have applied the MDSC technique for the study of kinetics of crystallization of Fe-based bulk metallic glass. The detailed crystallization of the present system, namely $Fe_{67}Co_{18}B_{14}Si_1$ using DSC has already been reported by us [18]. Hence, we thought it worthwhile to investigate the crystallization of this system in MDSC and to study the applicability of various kinetic equations utilized for linear heating in normal DSC.

2. Theory

Sensitivity and resolution are two important parameters associated with obtaining precise and accurate DSC results. Generally, optimizing both of these parameters simultaneously is difficult because sensitivity is increased by larger sample size and faster heating rates, while resolution is improved by smaller sample sizes and slower heating rates. MDSC employs same heat flux DSC cell arrangement, however, with a different and more complex heating profile applied to sample and reference. The heating profile is obtained by superimposing a sinusoidal modulation on the linear heating ramp where sample temperature increases continuously with time but not linearly, thus apparently, having an effect as if two experiments were running simultaneously; one traditional linear heating and other sinusoidal heating. These two simultaneous experiments depend on three operational parameters viz. underlying heating rate (β), period of modulation (p) and amplitude of temperature modulation (A_T). The slower linear heating rate results in improvement in resolution and the faster sinusoidal heating rate improves the sensitivity in the same experiment. Thus, major advantage of MDSC is increase in resolution without compromising the sensitivity [19].

Fourier transformation of modulated heat flow will give the value of an average heat flow, which is equivalent to the 'total' heat in conventional DSC. The ratio of the modulated heat flow amplitude and modulated heating rate amplitude will give heat capacity; and the reversing heat flow is product of heat capacity and the average heating rate whereas non-reversing heat flow is the difference between the 'total' heat flow and reversing heat flows. The separation of the 'total' heat flow into its reversing and non-reversing component is based on the changes occurring in the measured heat capacity rather than 'thermodynamical reversibility'.

The sample temperature is modulated sinusoidally about a constant ramp and sample temperature T at any time t is

$$T(t) = T_o + \beta t + A_T \sin(\omega t)$$

$$\alpha = \frac{dT}{dt} = \beta + A_T \omega \cos(\omega t)$$

where T_o is the initial temperature, β the heating rate, A_T amplitude of temperature modulation and p the period in second. It is very essential to have positive heating profile through out the MDSC experiment. To achieve this and to avoid cooling, following condition must be satisfied

$$\beta \geq A_T \frac{2\pi}{p}$$

The apparatus measures the total heat flow, which primarily is the amplitude of the instantaneous heat flow and average heat flow. The instantaneous heat flow is given by

$$\frac{dQ}{dt} = C_p(\beta + A_T \omega \cos(\omega t)) + f'(t, T) + A_K \sin(\omega t)$$

where $(\beta + A_T \omega \cos(\omega t))$ is the measured heating rate (dT/dt), $f'(t, T)$ the kinetic response without temperature

modulation and A_K the amplitude of kinetic response to temperature modulation. Deconvolution of the signals in MDSC separates the 'total' heat flow into its heat capacity related (reversing) and kinetic (non-reversing) components.

The determination of mechanism of crystallization is of paramount importance for the determination of the activation energy of crystal growth from MDSC data. The purpose of present study is to apply MDSC to ascertain the mechanism of crystallization.

3. Experimental

The metallic glass samples of $Fe_{67}Co_{18}B_{14}Si_1$ (2605CO) were procured from Allied Corporation (USA). They were in the form of continuous ribbon 2.5 cm wide and 30 μm thick. The samples were prepared by the melt spinning technique. The crystallization kinetics of this glassy alloy is studied using DSC 2910 (TA Instruments Inc., USA) system. The samples were heated with various heating rates to study non-isothermal kinetics. The crystallization fractions at various temperatures and various heating rates were obtained from the crystallization curves at different heating rates. Unlike the conventional DSC, a non-linear heating was employed by superposition of a sinusoidal temperature modulation on a linear heating.

4. Results and discussion

Fig. 1 shows a typical MDSC thermogram of $Fe_{67}Co_{18}B_{14}Si_1$ glass at an average heating rate of 4 °C/min. The amplitude of temperature modulation has been calculated through the following equation:

$$A_T < \frac{\beta}{2\pi} p$$

In fact, A_T has been taken to be just slightly less than $(\beta/2\pi)p$. This is required due to two reasons. Firstly, by taking $A_T < (\beta/2\pi)p$, the instantaneous heating rate $\alpha = \beta + A_{T\omega}\cos(\omega)$ is always positive. Thus, material is not cooled at any time during modulation, eliminating the possibility of artificially affecting any crystallization process. Secondly, by keeping the average heating rate close to zero, there is almost no heat flow associated with the heat capacity related (reversing events) and hence any heat flow observed must be the result of kinetic phenomena. Consequently, this condition permits continuous time-dependent processes such as crystal perfection or crystallization to be observed in the raw, modulated heat flow signal.

The fractional crystallization (x) data from the DSC can be fitted to KJMA equation to derive the kinetic parameters n, E_c and K_0. The main assumptions involved in KJMA

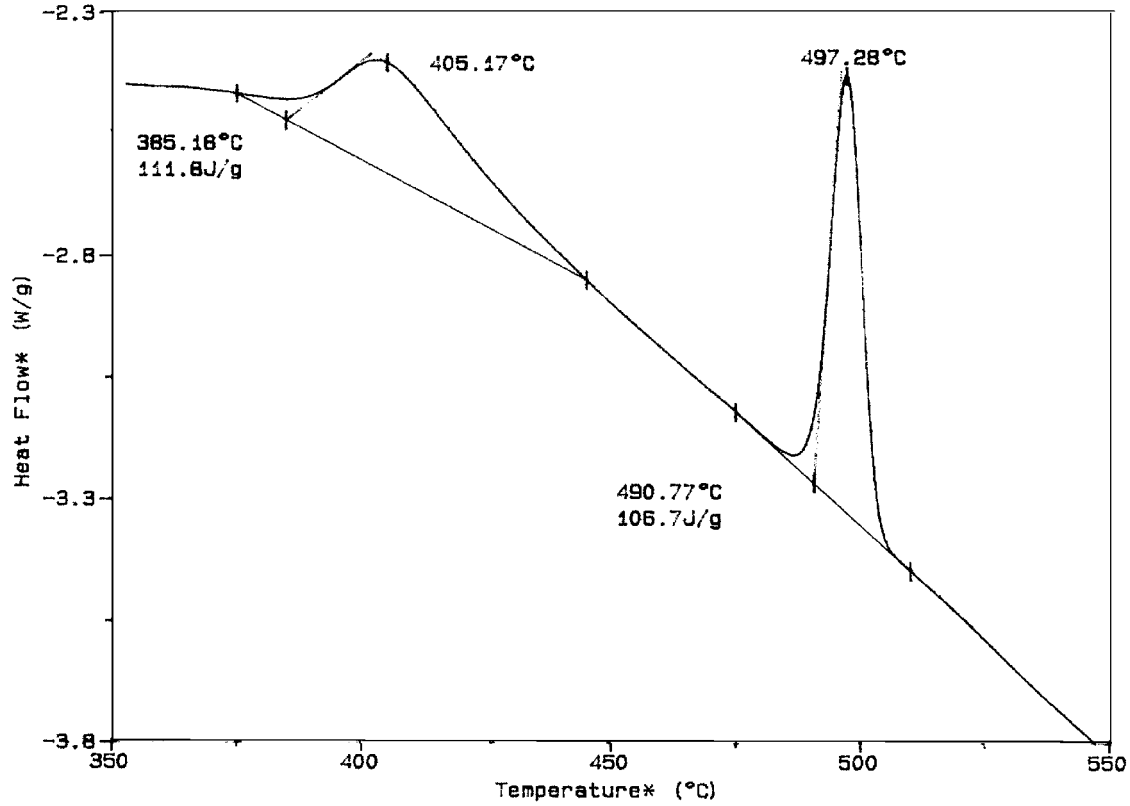

Fig. 1. MDSC thermogram of $Fe_{67}Co_{18}B_{14}Si_1$ glass at a heating rate of 4 °C/min.

approach [20–24] are:

(1) The crystallization data follow the iso-kinetic model:

$$\frac{dx}{dt} = K(T)\,f(x) \tag{1}$$

(2) The rate constant is assumed to show Arrhenius temperature dependence:

$$K(T) = K_0 \exp\left[\frac{-E_c}{RT}\right] \tag{2}$$

(3) KJMA simplest case equation is

$$f(x) = n(1-x)[-\ln(1-x)]^{(n-1)/n} \tag{3}$$

The overall assumptions lead to

$$[-\ln(1-x)]^{1/n} = K_0 \int_0^t \exp\left(-\frac{E_c}{RT}\right) dt \tag{4}$$

where n is the Avrami exponent and E_c the activation energy. Eq. (4) can be written as

$$x = 1 - \exp\left[\frac{-K_0}{\alpha}\int_{T_0}^{T} \exp\left(\frac{-E_c}{RT}\right) dT\right]^n \tag{5}$$

where T_o is onset crystallization temperature.

However, we do not get unique values of n as three fitting parameters, viz. n, k_0 and activation energy E are involved. Simultaneous determination of all kinetic parameters from a single non-isothermal experiment is quite problematic as observed by Kemeny and Sestak [25].

The experimental data for non-isothermal crystallization has been independently interpreted on the basis of method of modified Kissinger's equation [26] for determination of activation energy and fractional crystallization method [27] for ascertaining mechanism. From the equation suggested by Matusita and Sakka for non-isothermal crystallization, the activation energy for crystallization, E_c, can be evaluated:

$$\ln[-\ln(1-x)] = -n\ln(\alpha) + 6\ln T - \frac{mE_c}{RT} + \text{Const.} \tag{6}$$

where x is the fractional crystallization, at any temperature T and α is heating rate. The equation of Matusita and Sakka given by Eq. (6) originates from the following expression:

$$[-\ln(1-x)] = \frac{k'T^6}{\alpha^n}\exp\left(-\frac{mE_c}{RT}\right) \tag{7}$$

For MDSC, the measured heating rate becomes

$$\alpha = \frac{dT}{dt} = \beta + A_T\omega\cos(\omega t) \tag{8}$$

Here, β is the linear rate and the second term comes from sinusoidal temperature modulation.

Thus, the expression (9) changes to

$$[-\ln(1-x)] = \frac{k'T^6}{(\beta + A_T\omega\cos\omega t)^n}\exp\left(-\frac{mE_c}{RT}\right)$$

$$\ln[-\ln(1-x)] = -\ln(\beta + A_T\omega\cos\omega t)^n + 6\ln T - \frac{mE_c}{RT} + \text{Const.}$$

Further simplification leads to

$$\ln[-\ln(1-x)] = -n\ln\beta - n\ln\left(1 + \frac{A_T\omega}{\beta}\cos\omega t\right) + 6\ln T - \frac{mE_c}{RT} + C \tag{9}$$

Assuming $|(A_T\omega/\beta)\cos\omega t| < 1$ we can expand the second logarithm term on RHS of Eq. (9) as

$$\ln\left(1 + \frac{A_T\omega}{\beta}\cos\omega t\right) = \frac{A_T\omega}{\beta}\cos\omega t - \frac{A_T^2\omega^2}{2\beta^2}\cos^2\omega t + \cdots \tag{10}$$

neglecting the higher order terms. Then, Eq. (9) can be written as

$$\ln[-\ln(1-x)] = -n\ln\beta - n\left\{\frac{A_T\omega}{\beta}\cos\omega t - \frac{A_T^2\omega^2}{2\beta^2}\cos^2\omega t + \cdots\right\} + 6\ln T - \frac{mE_c}{RT} + C \tag{11}$$

Taking the average over a complete cycle,

$$\ln[-\ln(1-x)] = -n\ln\beta + \frac{A_T^2\omega^2}{2\beta^2}\frac{1}{2} + 6\ln T - \frac{mE_c}{RT} + C = -\ln\beta\left\{n - \frac{nA_T^2\omega^2}{4\beta^2}\right\} + 6\ln T - \frac{mE_c}{RT} + C \tag{12}$$

For one-, two- or three-dimensional nucleation, the value of the exponent n is expected to be more as compared to the subsequent value obtained from DSC results because the value of $\ln\beta$ in the denominator of the second term within parenthesis on RHS of Eq. (12) is always negative. Let us call this as Avrami exponent and denote it as n'.

For the evaluation of the apparent Avrami parameter n', $\ln[-\ln(1-x)]$ was plotted as a function of $\ln(\alpha)$ for DSC and $\ln(\beta)$ for MDSC. The dimensionality can be derived from the apparent Avrami exponent n' by using the expression

$$n' = a + bm' \tag{13}$$

where $a = 1$ for constant nucleation rate, $a = 0$ for zero nucleation rate, and $a > 1$ for increasing nucleation rate, $m' = 1$ for one-dimensional growth, $m' = 2$ for two-dimensional growth and $m' = 3$ for three-dimensional growth.

m' has been termed as apparent value of dimensionality. The plots of $\ln[-\ln(1-x)]$ as a function of $\ln(\alpha)$ and $\ln(\beta)$ for the two steps of the crystallization for DSC and MDSC are shown in Figs. 2 and 3, respectively. The derived values

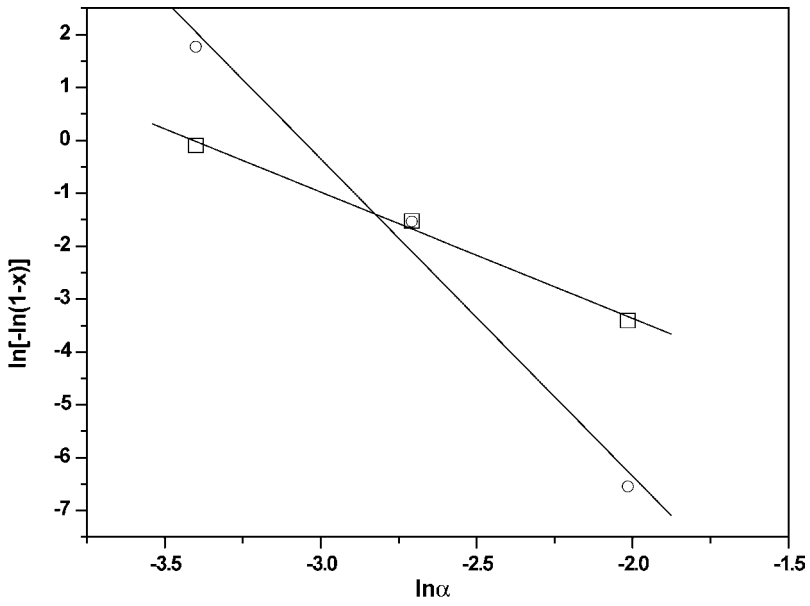

Fig. 2. Plot of $\ln[-\ln(1-x)]$ vs. $\ln(\alpha)$ for DSC: (□) first peak at $T = 673$ K; (○) second peak at $T = 668$ K.

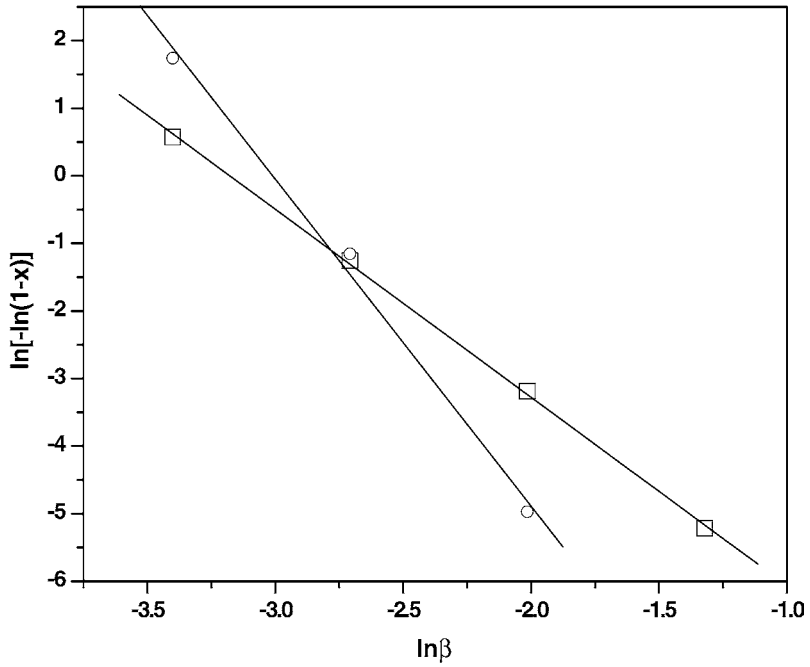

Fig. 3. Plot of $\ln[-\ln(1-x)]$ vs. $\ln(\beta)$ for MDSC: (□) first peak at $T = 673$ K; (○) second peak at $T = 768$ K.

of Avrami exponent for two steps of crystallization using both DSC and modulated DSC have been given in Table 1. It is obvious that the n' values for both the steps are not identical for DSC and MDSC experiments. For the first step crystallization, the n' (2.78) from MDSC comes out to be higher than the n' obtained (2.38) from DSC plot. But, for second step crystallization, the n' derived (4.84) from MDSC plot is lower than the corresponding value (5.99) of DSC. So, it appears from this that one is not justified in taking average over a complete cycle which leads to Eq. (12). Instead, one should note down the initial temperature T_o and plot the

Table 1
Apparent values of the Avrami exponent (n') and the dimensionality of growth (m') obtained from the plots in Figs. 2 and 3

Crystallization peak	n'			m'
	Present results	[29]	[28]	
DSC				
First	2.38 ± 0.18	1.00	2.00	2.76 ± 0.18
Second	5.99 ± 0.71	1.55	2.8	4.99 ± 0.71
MDSC				
First	2.78 ± 0.05	–	–	3.56 ± 0.05
Second	4.84 ± 0.38	–	–	3.84 ± 0.38

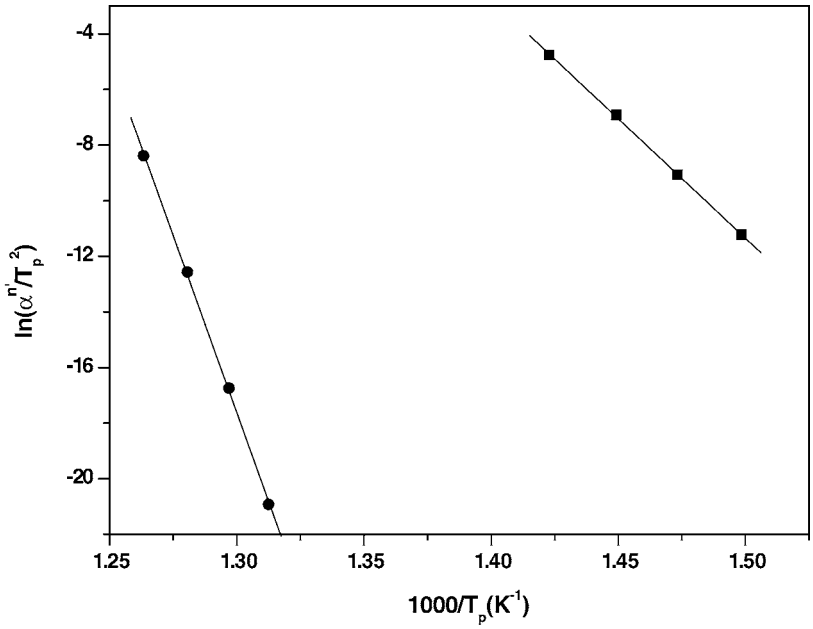

Fig. 4. Plot of $\ln[\alpha^n / T_p^2]$ vs. $1/T_p$ for DSC: (■) first peak; (●) second peak.

graph of time and temperature following the equation:

$$T(t) = T_0 + \beta t + A_T \sin(\omega t)$$

From the resulting plot, one can get time t corresponding to a particular temperature of interest T and putting the same t in Eq. (11) one may get a correct estimate of n'. The values of n' for the two stages of crystallization from literature [28,29] have also been listed in the table for comparison. It can be observed from Table 1 that in the present work, the first step of crystallization (primary crystallization) is a diffusion-controlled process with constant nucleation rate ($a = 1$). Our observation for primary crystallization is consistent with the isothermal DSC studies of Baburaj et al. [28]. de Biasi and Grillo [29], on the other hand, get Avrami exponent $n = 1$ suggesting that primary crystallization is diffusion-controlled process with a nucleation rate close to zero.

The second step polymorphic crystallization is found to be an interface-controlled growth similar to the observations

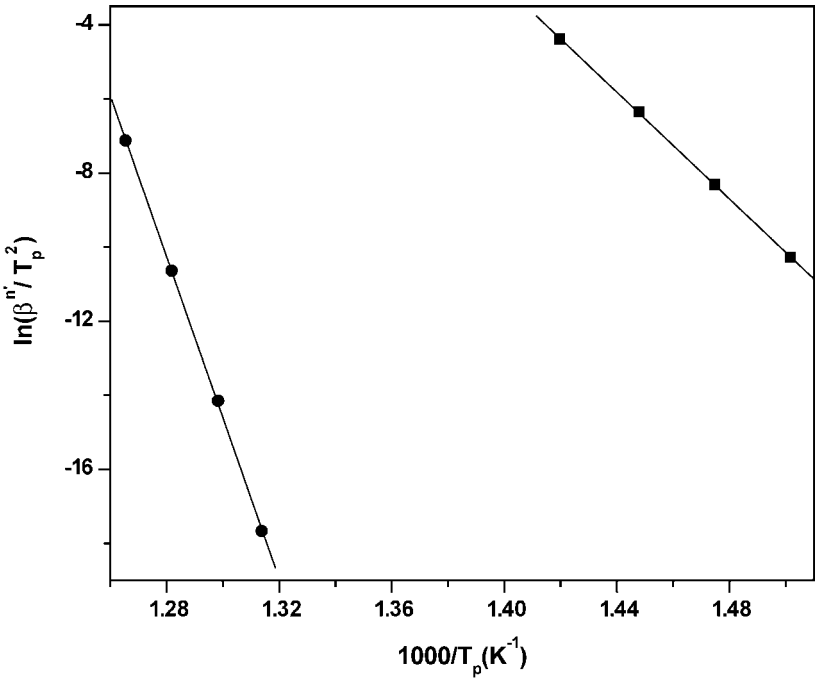

Fig. 5. Plot of $\ln[\beta^n / T_p^2]$ vs. $1/T_p$ for MDSC: (■) first peak; (●) second peak.

Table 2
mE_c and E_c values obtained from the plots in Figs. 4 and 5

Crystallization peak	mE_c/R	mE_c (kJ/mol)	E_c (kJ/mol)			
			Present results	[29]	[28]	[33][a]
DSC						
First	85.98 ± 0.99	714 ± 8	258 ± 13	230	231	260
Second	255.19 ± 4.25	2120 ± 35	424 ± 53	365	360	394
MDSC						
First	72.02 ± 0.56	598 ± 4	168 ± 3	–	–	–
Second	217.44 ± 2.16	1806 ± 17	470 ± 42	–	–	–

[a] For $Fe_{65}Co_{18}B_{16}Si_1$.

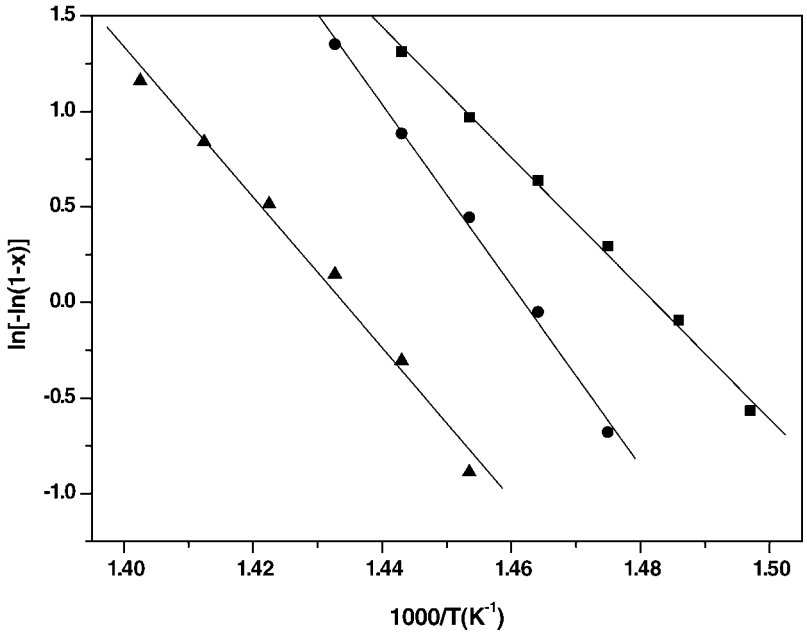

Fig. 6. Plot of $\ln[-\ln(1-x)]$ vs. $1/T$ for DSC first peak: (■) 2 °C/min; (●) 4 °C/min; (▲) 8 °C/min.

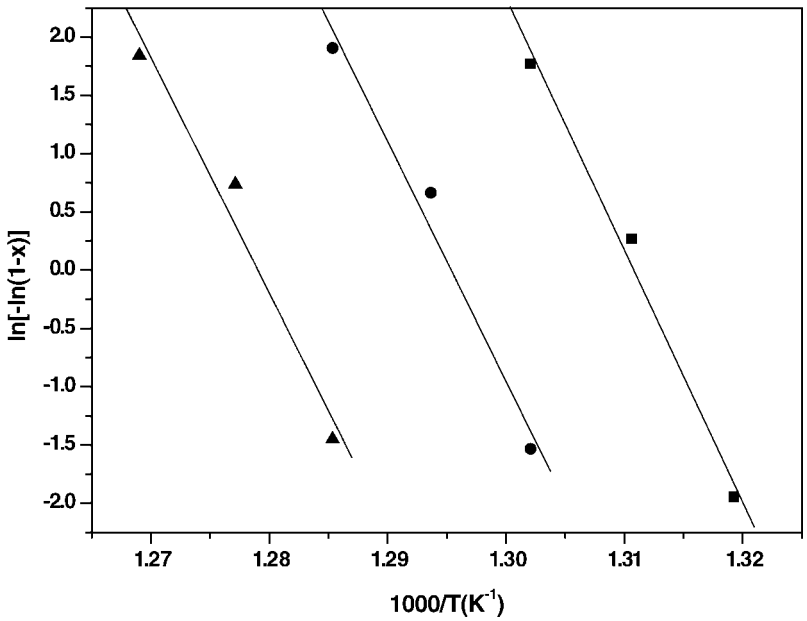

Fig. 7. Plot of $\ln[-\ln(1-x)]$ vs. $1/T$ for DSC second peak: (■) 2 °C/min; (●) 4 °C/min; (▲) 8 °C/min.

Table 3
mE_c and m values obtained from the plot of $\ln[-\ln(1-x)]$ vs. $1/T$ at different heating rates for DSC

Heating rate (°C/min)	mE_c/R	mE_c (kJ/mol)	m
First peak			
2	34.21 ± 0.99	284 ± 8	1.10 ± 0.02
4	47.29 ± 1.74	393 ± 14	1.52 ± 0.02
8	39.39 ± 2.22	327 ± 18	1.27 ± 0.01
Second peak			
2	216.41 ± 23.08	1798 ± 191	4.23 ± 0.08
4	205.69 ± 32.07	1709 ± 266	4.02 ± 0.12
8	202.15 ± 37.38	1679 ± 310	3.95 ± 0.23

of Baburaj et al. [28]. However, de Biasi and Grillo [29] get quite low value of n (= 1.55) for second step indicating it to be diffusion-controlled process with a constant nucleation rate. The apparent Avrami exponent's values for polymorphic crystallization, in the present study, indicating interface-controlled growth, come out to be higher than that obtained by Baburaj et al. [28]. Normally, n' should not exceed 4 (i.e. the value for three-dimensional bulk nucleation). But, in the present study, its value is higher than 4. $n' > 4$ indicates that the three-dimensional interface-controlled crystallization takes place with increased nucleation rate. Similar high values of n (i.e. $n = 6$) have been reported for a ternary chalcogenide glass [30]. For the evaluation of the apparent dimensionality of growth, m', Eq. (13) has been used, assuming diffusion-controlled growth for primary crystallization and interface-controlled growth for polymorphic crystallization and the so-obtained values have been provided in Table 1.

For the evaluation of apparent activation energy of crystallization E_c, the modified Kissinger equation [26] is used and is given by the following expression:

$$\ln\left(\frac{\alpha^{n'}}{T_p^2}\right) = -\frac{m'E_c}{RT_p} + 4\ln T_p + \ln K \tag{14}$$

where the shift in peak crystallization temperature, T_p, with heating rate α is used to determine E_c and m' is the apparent dimensionally of growth.

In temperature modulated DSC, the measured heating rate is non-linear given by Eq. (8). Putting $\alpha = \beta + A_T\omega\cos(\omega t)$ in the modified Kissinger equation (Eq. (14)), we get

$$\ln\left(\frac{\beta^{n'}}{T_p^2}\right) + \ln\left(1 + \frac{A_T\omega}{\beta}\cos\omega t\right)^{n'} = -\frac{m'E_c}{RT_p} + 4\ln T_p + \ln K$$

$$\ln\left(\frac{\beta^{n'}}{T_p^2}\right) + n'\left(\frac{A_T\omega}{\beta}\cos\omega t - \frac{A_T^2\omega^2}{2\beta^2}\cos^2\omega t + \cdots\right) = -\frac{m'E_c}{RT_p} + 4\ln T_p + \ln K$$

Taking the average over a complete cycle, we get

$$\ln\left(\frac{\beta^{n'}}{T_p^2}\right) - \frac{n'A_T^2\omega^2}{4\beta^2} = -\frac{m'E_c}{RT_p} + 4\ln T_p + \ln K \tag{15}$$

where β is linear heating rate. The second term on the LHS of Eq. (15) is expected to cause non-linearity in the modified Kissinger plot of modulated DSC results. However, it is observed that the points of $\ln(\beta^{n'}/T_p^2)$ versus $1/T_p$ lie on straight line. So, we have not considered the effect of

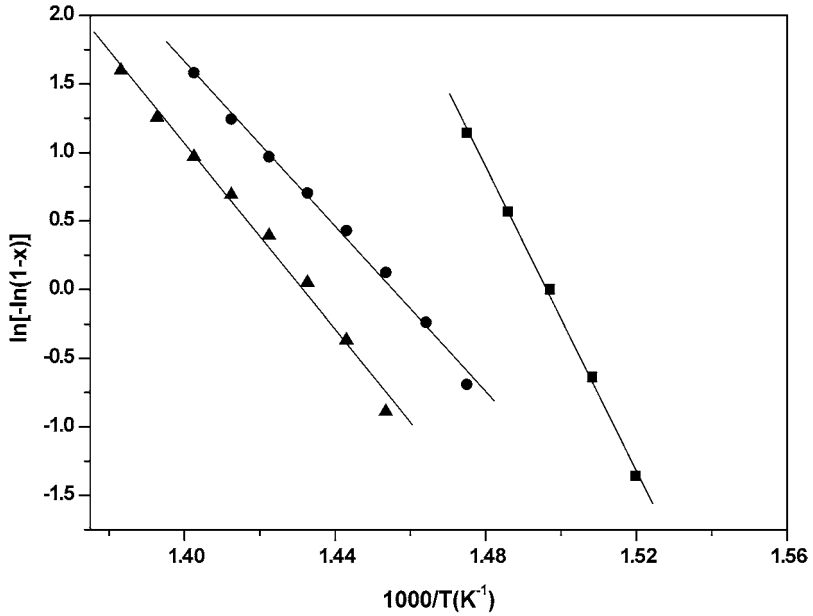

Fig. 8. Plot of $\ln[-\ln(1-x)]$ vs. $1/T$ for MDSC first peak: (■) 2 °C/min; (●) 4 °C/min; (▲) 8 °C/min.

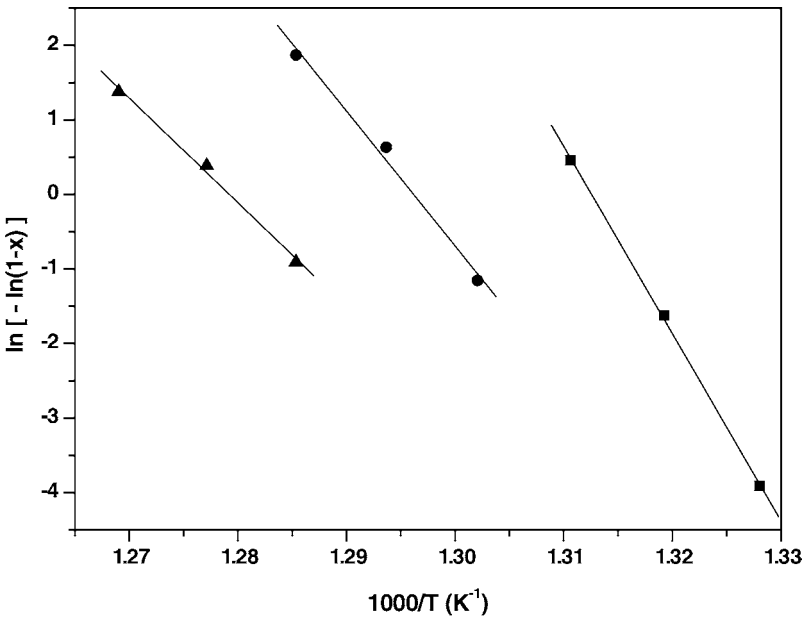

Fig. 9. Plot of $\ln[-\ln(1-x)]$ vs. $1/T$ for MDSC second peak: (■) 2 °C/min; (●) 4 °C/min; (▲) 8 °C/min.

the second term. The activation energy of crystallization obtained in such a way is termed as apparent activation energy.

Using the value of the apparent order parameter n' and m', E_c, the apparent activation energy of crystallization is computed from the slope of $\ln(\beta^{n'}/T_p^2)$ versus $1/T_p$ plots for first and second crystallization processes using DSC and MDSC shown in Figs. 4 and 5, respectively. The values of activation energy for DSC and MDSC derived for two-step crystallization are given in Table 2. Within the errors indicated in the table, out data is in fair agreement with the reported values in the literature.

From the slope of the $\ln[-\ln(1-x)]$ versus $1/T$ data mE_c was calculated using Eq. (8). It is well known that a double logarithm function in general, is not very sensitive to subtle changes to its argument. Therefore, one can expect that the plots of $\ln[-\ln(1-x)]$ versus $1/T$ may be linear even in the case the JMA model is not fulfilled [31]. In fact, the plot has been found to be linear over most of the temperature range. The curvature of such plot comes from either in the beginning of the crystallization (lower T values) or near the completion of the crystallization (higher T values). The non-linearity at lower T values is due to increased inaccuracy in the evaluation of fractional crystallization x at lower temperature [32]. Generally, the break in the slope in the plot of $\ln[-\ln(1-x)]$ versus $1/T$ at high temperatures, i.e. at low value of 1/T is attributed to the saturation of the nucleation sites in final stages of the crystallization or to the restriction to the crystal growth by the small size of the particles [30].

The mE_c values were observed to be more or less heating rate independent in the case of plots obtained from DSC curves drawn for both first step of crystallization (Fig. 6) and for second stage crystallization (Fig. 7). This is obvious from the various mE_c values derived from the plots. Consequently, the dimensionality of growth m also becomes heating rate independent. The m values for the two crystallization steps using both DSC and MDSC data have been listed in Table 3.

The MDSC plots, on the other hand, shown in Figs. 8 and 9 clearly point out the heating rate dependent nature of crystallization process observed in MDSC. This leads to variable values of the dimensionality of growth m for different heating rates (Table 4) for both the stages of crystallization. The m values decrease with increasing heating rate. Similar heating rate dependence of m has been observed by Matusita and Sakka [27] also.

The relative error in the evaluated mE_c from MDSC technique is found to be smaller as compared to DSC method. This may be attributed to the sinusoidal temperature modulation, which leads to longer experimental time than conventional DSC experiments allowing the system to equilibrate causing uniform mechanism of crystallization at all heating rates.

Finally, a comparative plot of the thermograms at various heating rates for both DSC and MDSC shown in Fig. 10 is indicative of the fact that the MDSC has increased sensitiv-

Table 4
mE_c and m values obtained from the plot of $\ln[-\ln(1-x)]$ vs. $1/T$ at different heating rates for MDSC

Heating rate (°C/min)	mE_c/R	mE_c (kJ/mol)	m
First peak			
2	55.44 ± 1.37	460 ± 11	2.74 ± 0.02
4	30.08 ± 0.91	250 ± 7	1.48 ± 0.02
8	33.89 ± 1.31	281 ± 11	1.67 ± 0.03
Second peak			
2	251.10 ± 5.86	2086 ± 48	4.43 ± 0.29
4	180.92 ± 18.32	1503 ± 152	3.19 ± 0.04
8	140.17 ± 10.08	1164 ± 83	2.48 ± 0.04

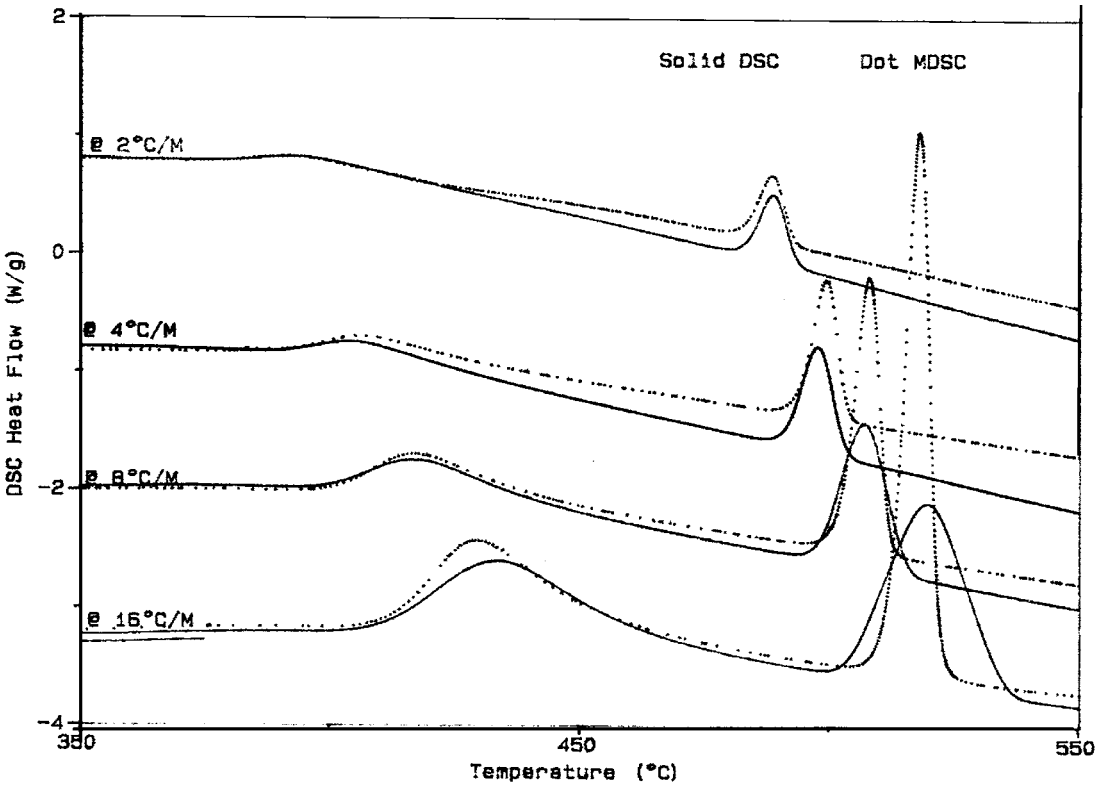

Fig. 10. DSC and MDSC thermograms for various heating rates.

ity for transition-like crystallization. This is clear from the increased sharpness of the crystallization peaks as compared to DSC peaks at all heating rates.

5. Conclusion

The crystallization kinetics of $Fe_{67}Co_{18}B_{14}Si_1$ glass has been investigated using both DSC and modulated DSC techniques. As such both of them take good account of the two-step crystallization of this multicomponent amorphous alloy. The first step corresponds to diffusion-controlled primary crystallization, while the second step is exhibited as a polymorphic interface-controlled crystallization process with increased nucleation rate. These features are in line with the other reported literature. Although kinetic equations get somewhat more involved and complicated in MDSC, the smaller relative error in evaluation of kinetic parameters like activation energy as compared to DSC is an encouraging sign. Further, the modulated DSC seems to be more sensitive to the transition-like crystallization.

Acknowledgements

The authors are thankful to the esteemed referees for critical evaluation of the manuscript and also for enlightening suggestions. The authors are grateful to IUC for DAE facilities at Indore for providing the modulated DSC equipment for carrying out the present work.

References

[1] F.E. Luborsky (Ed.), Amorphous Metallic Alloys, Butterworths, Boston, 1983.
[2] T.R. Anantharaman (Ed.), Metallic Glasses: Production, Properties and Applications, Trans. Tech., Switzerland, 1984.
[3] S. Steeb, H. Worlimont (Eds.), Rapidly Quenched Metals, North-Holland, Amsterdam, 1985.
[4] R.W. Cochrane, J.O. Strom-Olsen (Eds.), Rapidly Quenched Metals 6, Mater. Sci. Eng. 97–99 (1988).
[5] P. Tomic, M. Davidovic, J. Non-Cryst. Solids 204 (1996) 32.
[6] A.K. Galwey, Thermochim. Acta 399 (2003) 1.
[7] S.D. Kaloshkin, I.A. Tomilin, Thermochim. Acta 280–281 (1996) 303.
[8] M. Reading, A. Luget, R. Wilson, Thermochim. Acta 239 (1994) 295.
[9] M. Reading, et al., US Patent 5,224,775 (1993).
[10] P.S. Gill, S.R. Sauerbrunn, M. Reading, J. Therm. Anal. 40 (1993) 931.
[11] S.X. Xu, Y. Li, Y.P. Feng, Thermochim. Acta 343 (2000) 81.
[12] J. Cao, Thermochim. Acta 325 (1999) 89.
[13] J. Cao, Thermochim. Acta 325 (1999) 101.
[14] A. Boller, C. Schich, B. Wunderlich, Thermochim. Acta 266 (1995) 97.
[15] T. Wagner, S.O. Kasap, Phil. Mag. B 74 (1997) 667.
[16] Y. Li, S.C. Ng, Z.P. Lu, Y.P. Feng, K. Lu, Phil. Mag. Lett. 78 (1998) 213.
[17] A. Pratap, K.G. Raval, A.M. Awasthi, Mater. Sci. Eng. A 304–306 (2001) 357.

[18] A. Pratap, K.G. Raval, A. Gupta, S.K. Kulkarni, Bull. Mater. Sci. 23 (2000) 185.
[19] Modulated DSC™ Compendium: Basic Theory and Experimental Considerations, TA Instruments Inc., New Castle, DE, USA, TA-210.
[20] N. Kolmogorov, Bull. Acad. Sci. USSR Phys. Ser. 1 (1937) 355.
[21] W.A. Johnson, P.A. Mehl, Trans. Inst. Min. Metall. Pet. Eng. 135 (1939) 416.
[22] M. Avrami, J. Chem. Phys. 7 (1939) 1103.
[23] M. Avrami, J. Chem. Phys. 8 (1940) 212.
[24] M. Avrami, J. Chem. Phys. 9 (1941) 177.
[25] T. Kemeny, J. Sestak, Thermochim. Acta 110 (1978) 113.
[26] K. Matusita, S. Sakka, J. Non-Cryst. Solids 38–39 (1980) 741.
[27] K. Matusita, S. Sakka, Phys. Chem. Glasses 20 (1979) 81.
[28] E.G. Baburaj, G.K. Dey, M.J. Patni, R. Krishnan, Scripta Metall. 19 (1985) 305.
[29] R.S. de Biasi, M.L.N. Grillo, J. Alloys Compd. 279 (1998) 233.
[30] S. Mahadeven, A. Giridhar, A.K. Singh, J. Non-Cryst. Solids 88 (1986) 11.
[31] J. Malek, Thermochim. Acta 267 (1995) 61.
[32] N. Clavaguera, M.T. Clavaguera-Mora, M. Fontana, J. Mater. Res. 13 (1998) 744.
[33] M.D. Baro, S. Surinach, J.A. Diego, M.T. Clavaguera-Mora, Mater. Sci. Eng. A 133 (1991) 807.